Attempt to correlate dislocations network and distribution to macroscale plane rotations in cast-mono ingots

Etienne Pihan, Mickael Albaric, Gabrielle Regula, Nathalie Mangelinck-Noël

Attempt to correlate dislocations network and distribution to macroscale plane rotations in <001> cast-mono ingots

Etienne Pihan[*1], Mickael Albaric[1], Gabrielle Regula[2], Nathalie Mangelinck-Noël[2]

[1]Univ. Grenoble Alpes, CEA, Liten, Campus Ines, 73375 Le Bourget du Lac, France
[2]Aix Marseille Univ, Université de Toulon, CNRS, IM2NP, Marseille, France

*Corresponding author email address: etienne.pihan@cea.fr
Co-authors email addresses: mickael.albaric@cea.fr, gabrielle.regula@univ-amu.fr, nathalie.mangelinck@im2np.fr

Abstract

This work aims to contribute to the understanding of the mechanisms behind electrically active crystalline defect formation in cast-mono (cm) ingots grown along the <001> axis. Both the spatial distributions of background dislocations in the cellular dislocation array and the driving force for dislocation multiplication in the sub-grains are not perfectly understood. Macroscale length crystal rotations are here characterized by the (θ/2θ) X-ray diffraction (XRD) method at different ingot heights and along two perpendicular sample axes. XRD measurements show the presence of crystal rotations in the large single grain domain. Two orthogonal misorientations components are found to evolve linearly along each sample axis forming plane orientation gradients up to (0.05±0.02) degree/cm extending over 12 cm inside the cast-mono grain. (001) crystal structure deformation are also analysed by rocking curve imaging (RCI) using synchrotron radiation on wafers of a neighboring brick. First, results confirm the presence of the plane orientation gradient measured by XRD and its order of magnitude. Second, RCI results demonstrate that the plane orientation gradient is associated to the cellular dislocation network. Therefore, these results strongly suggest that background dislocations network of a cellular form can create an organized orientation gradient at large distance within the ingot. The involvement of the characterized orientation gradients in the formation and extension of electrically active SGBs in cast-mono ingots is discussed.

Keywords

silicon, cast-mono, dislocations, crystal orientation, X-ray diffraction, sub-grain boundaries

Highlights

- Crystal structure deformation measurements of cm-Si ingots.
- Evidence of the presence of {001} planes orientation gradients.
- Plane orientation gradients almost constant along the sample axes.
- Orientation gradients increase with the ingot height.
- Orientation gradients associated to the cellular network of dislocations.

1. Introduction

In the cast-mono silicon (cm-Si) process, a pavement of monocrystalline seeds is placed at the bottom of the crucible in order to take up the initial orientation of the seeds [1, 2]. Efficiencies measured on cm-Si were first limited due to the presence of structural defects such as parasitic grain nucleation on the walls of the crucible [3, 4] generally by twin formation. Nowadays, the main issue that remains is the control of structural defects like dislocations that can lead to the downgrading of the wafers. Indeed, thanks to seeding, cm-Si shows improved properties [1], but an inhomogeneous distribution of dislocation clusters often results from the contact boundaries of the seed plates [3, 5, 6]. Dislocations can be either arranged in cellular patterns, in the entire cm-Si ingot and are known as background dislocations [5] or generated on the top of the seeds [7, 8], at their junctions on precipitates [7] and propagate vertically along the growth direction [3, 9, 10, 11, 12, 13] generating the formation of sub-grain boundaries (SGBs).

In a cm-Si ingot, dislocation cells and SGBs are inserted inside a giant grain generated by the use of large monocrystalline seeds (often larger than 150 x 150 mm^2 surface) making difficult by any characterization technique to cover the wide range of spatial dimensions (from dislocations to grains).

Two dislocation structures are characterized in <001> cm-Si material: a cellular network and complex tilt boundary domains. They differ drastically in terms of electrical activity, which is a major concern for photovoltaic (PV) application. The cellular structure is present in high carrier lifetime areas [14] and the complex tilt boundary structure (SGBs) is present in poor carrier lifetime areas [15]. The latter is detected by characterization techniques probing the carrier lifetime such as microwave photoconductance decay (MW-PCD) or photoluminescence (PL) imaging. This is most likely due to the difference of several orders in terms of dislocation density (much higher in sub-grains domains), and of the character of the dislocations.

Dislocations organized in cells and sometimes called background dislocations are either supposed to be associated to thermal gradients during heating and solidification [5] and/or could be frozen-in upon ingot cooling [16, 17]. As mentioned above, many local sources for SGBs have been found in the vicinity of the seeds and are systematically depicted as grown-in defects as they multiply along ingot height by increasing the total SGB length, the corresponding surface coverage and the tilt misorientation between subdomains. Lantreibecq *et al.* [18] have shown by stressing cm-Si samples *in situ* in a transmission electron microscope that isolated dislocations (a/2<110>{111} dislocation segments in the cell network) are as mobile as dislocations in Czochralski (Cz) ingots whereas edge type a/2<110> dislocations aligned vertically in SGBs are sessile. Nevertheless, unanswered questions remain, including: why dislocation density in cells is drastically reduced at the seed re-growth interface? Which driving force generates the new threading dislocations in SGBs? Indeed, the multiplication cause is unclear as there is no energy reduction if edge <110> dislocations result from two a/2<110> {111} dislocations by elastic reaction. Krause *et al.* [19] have shown that dense dislocation networks in cellular form in the seeds (far from side local sources) could result in sub-grains in the grown area and have correlated this area in seeds to (100) orientation tilt change measured by XRD. The origin of the tilts was attributed by the authors to stress-induced plastic deformation of the seeds, possibly originating from an uneven crucible bottom.

This work aims to contribute to the understanding of the mechanisms behind on the one hand, the dislocation network formation and on the other hand, the resulting electrically active crystalline defects in cast-mono ingots grown along the <001> axis. The dislocation array is correlated to the deformation measured by XRD, and the extension of the deformation to the grown volume is analysed. For that purpose, large scale (15.0 cm wide seed and grain) crystal

rotation is probed in the seeds. Additionally, those analyses are extended to the grown ingot to check if the crystal orientation is tilting. Rocking curve imaging (RCI) is carried out using synchrotron radiation on wafers of a neighboring brick to study the (001) rotation link with the dislocation networks.

2. Experimental methods

2.1. Cast mono samples

Ingots of various scales grown with the cast-mono process show that their edges are much more prone to defect multiplication with ingot height [6, 14, 17, 20]. For this study, the ingot is chosen because it has been extensively characterized [14, 15, 17, 18] and is representative of SGB multiplication along the height in side bricks which is an issue met and identified by industrials trying to develop cm-Si [21]. The cm-Si ingot used in this study is a 85 kg ingot grown with Cz seeds. The seed pavement is made of four 15.6 × 15.6 cm^2 main seeds with growth axis oriented in <001> ±2°. The saw damage layer resulting from the preparation of the seeds is removed by KOH etching. A quarter of this ingot has been precisely characterized by PL imaging, dislocation etch pit observation and SGB length measurements. The results and experimental details can be found in [17]. At brick scale, PL characterization reveals that electrically active SGBs mainly affect the quality of the top of the ingot.

In order to be able to measure an orientation tilt by X-ray (θ/2θ) method, areas of a cm-Si with no significant SGBs are required in order to be able to acquire a unique diffraction peak angular position. Three slabs from a brick A representing a quarter of ingot are used for XRD measurements (Figure 1.a). The initial Cz seeds orientation is <001> orientation normal to the surface with a precision better than 2° (standard PV specifications). A slab labelled S is chosen in the seed (ingot height H = 0.7 cm), another labelled SG at the start of growth (H = 1.4 cm) and the third one labelled HG close to half of total ingot height (H = 8.9 cm). At 8.9 cm height, the sub-grains cover less than 10% of the grain surface and are mainly positioned at ingot corners (opposite corner to the 0 reference in Figure 1.c) whereas no significant formed SGB can be detected by PL in the seed. Only a small area of SGBs is detected in the SG slab (Figure 1.b bottom right). Each slab is grinded before polishing and chemical attack is used to reveal dislocation etch pits. The brick D from the same ingot (Figure 1.a) is cut into wafers and characterized by rocking curve imaging to probe the different scales required for comparison of orientation tilts in the dislocation cell network [14] with the XRD measurements.

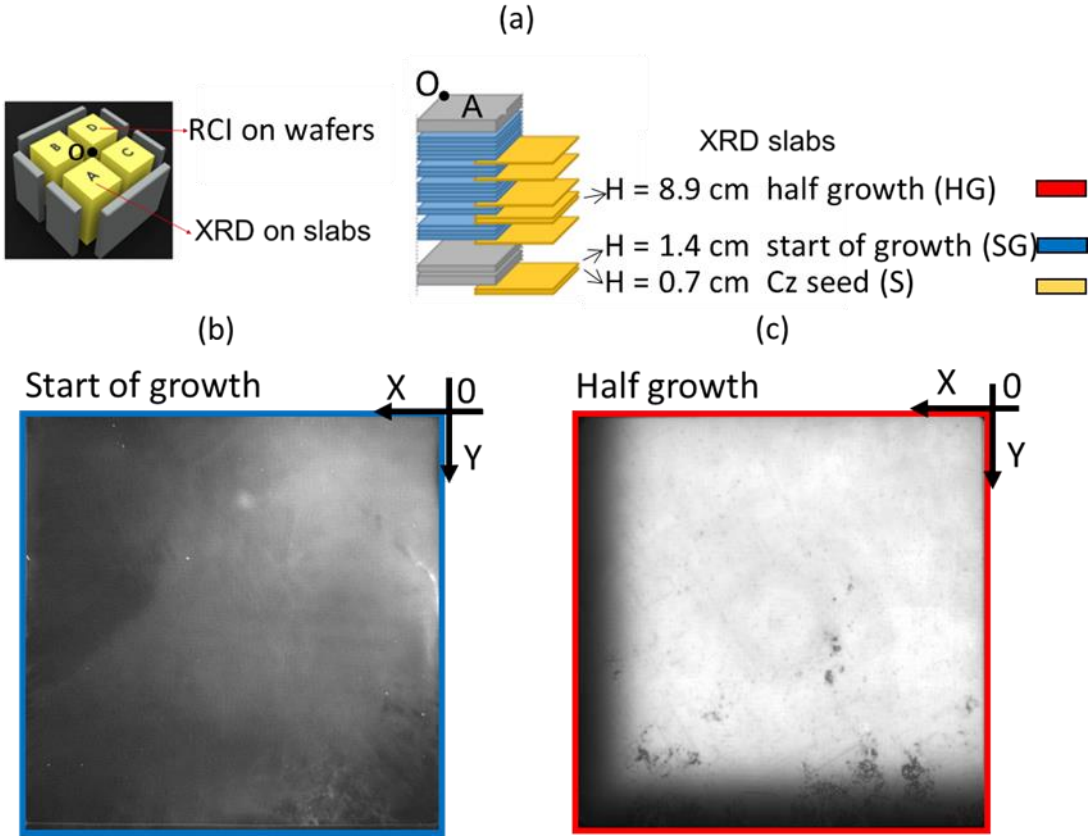

Figure 1: (a) Sketch of the 85 kg cm-Si ingot from which brick A is extracted for θ/2θ XRD measurements on three thick slabs cut at H = 0.7 cm, 1.4 cm, and 8.9 cm. Brick D is used for RCI analysis; Photoluminescence images of the 15.6 × 15.6 cm^2 samples for start of growth (SG) at H = 1.4 cm (b) and half ingot (HG) at H = 8.9 cm (c). Grey scale contrast of the PL images indicates higher (bright) and lower (darker) carrier lifetimes regions. The color legend red, blue and yellow in this paper, refers to half height (HG), start of growth (SG) and seed (S), respectively.

2.2. X-ray diffraction (θ/2θ) measurements

The deformation in cm-Si material is measured by X-ray diffraction (XRD) in θ/2θ configuration. Delta Technologies Int'l GMWS (550-300) equipment is used for a measurement of the misorientation with respect to the <001> crystallographic orientation along two X and Y sample axes (Figure 2).

The origin is taken at the ingot center (0 in Figures 1 and 2) and X and Y axes are named as depicted in Figure 2.b. According to the seed crystallographic orientation, X is deviated 30° from <110> direction as represented in Figure 2b. The slabs at H = 0.7 cm and 1.4 cm are in one 15.6×15.6 cm^2 piece and allow probing with our X-ray (θ/2θ) measurement system θ_x along the X-axis and θ_y along the Y-axis (Figure 2.a). The slab at 8.9 cm was cut into 25 squared 3.1×3.1 cm^2 sub-areas and is used to probe biaxial deformations θ_x and θ_y for X and Y axes. The nine squared sub-areas used in this study are shown in the image insert in Figure 2.b together with their schematic positions superimposed on the PL image of the sample. Macroscale-length crystal orientation rotations are extrapolated from the slopes of the local misorientation as a function of the distance in either X or Y axes. Altogether, the sample choice allows to probe <001> orientation tilts along two ingot axes (X and Y), seed / growth interface and tilts during growth.

As each slab is grinded prior to measurements, any orientation variation within a sample cannot be attributed to inaccurate flatness of the sample (flatness translated in angle is better than

0.01 degree). Nevertheless, a sample horizontal plane positioning error can exist for each sample compared to the others from both the slab cutting and the grinding step. Considering at maximum a difference of 200 µm on one side of the horizontal slab surfaces, we estimate the surface sample horizontal plane positioning to be better than 0.07 degree even in the worst case. Moreover, an error of the pre-positioning is possible depending mainly on the mechanics (including ball centering), of the order of 0.1 degree. A double measurement of each side after rotating the sample by 180 degrees eliminates this pre-positioning error δ. For this study, it was possible to reduce the error δ for all measurements on the HG sample thanks to sub-area geometry. An error of less than 0.05 degree is obtained for the HG sample and is lower than 0.1 degree in the case of full-size S and SG samples for which only one single measurement can be done per position.

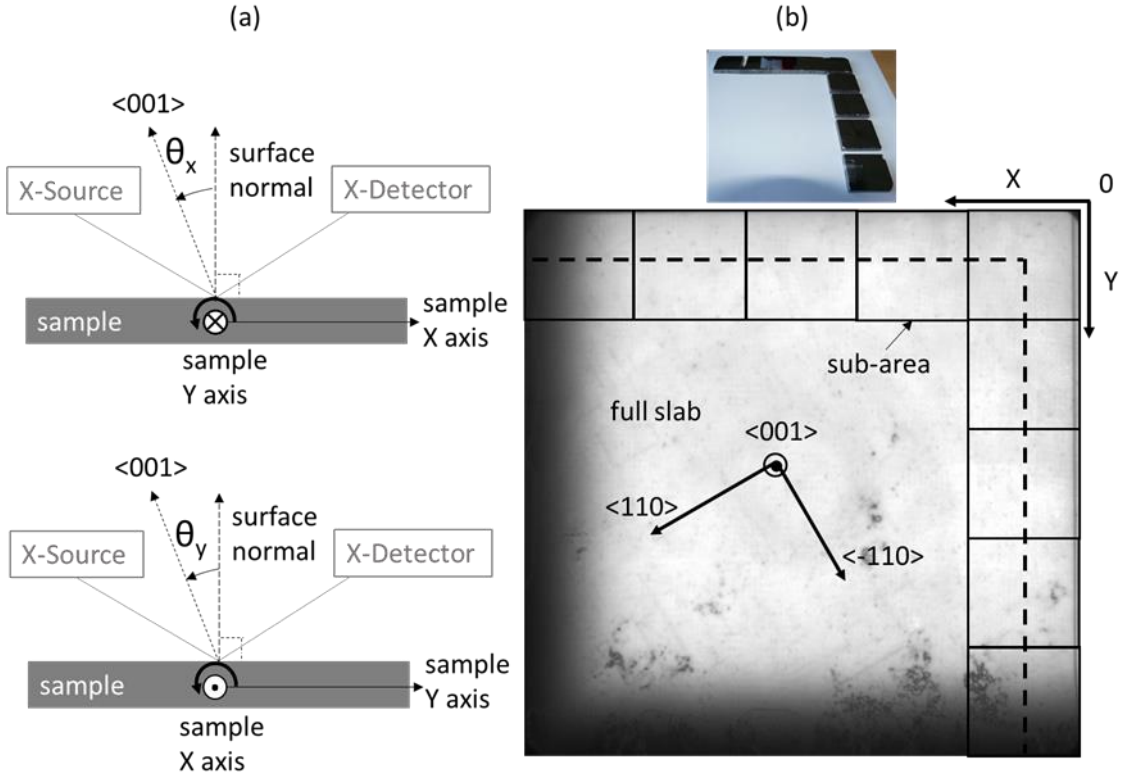

Figure 2: Sketch of θ_x and θ_y defined as the misorientation of {001} planes relatively to the sample surface normal (a), X and Y axes are taken along the edges of the 15.6 cm size slab with origin at the ingot center, and measurements are performed at (X, Y) positions at a distance of 1.5 cm from the edges (see dotted line) (b). θ_x and θ_y (X and Y directions, respectively) are measured for all samples.

2.3. Rocking curve imaging (RCI)

This technique can be interpreted as a fully quantitative version of X-ray topography [22]. The spatial distribution of the plane structure distortion can be visualized through a series of X-ray diffraction topographs recorded at successive rocking angles, which provides a rocking curve of each pixel of the image, from which maps of the integrated intensity, full width at half maximum (FWHM) and peak position (PP) can be generated. These maps measure the local plane distortion.

For rocking curve data acquisition, the wafer sample is positioned to diffract the Si (0 0 4) reflection in the horizontal scattering plane, and the diffracted beam images are recorded with

2.10^{-4} degree angular steps by using a CCD camera with optics giving a 1.87 µm image pixel size. The data are treated to extract the maps of integrated intensity and from a peak adjustment, the full width at half maximum (FWHM) and peak position (PP) for each pixel [23]. The peak position maps provide information on tilts and misorientations. Lattice parameter is assumed to remain homogeneous in the ingot and hence all peak position variations can be attributed to plane orientation tilts.

From the FWHM, the local density of non-geometrically necessary dislocations can be estimated from the Hirsch's formula [24]:

$$\rho = \frac{\beta^2}{9b^2} \quad (1)$$

where β is the FWHM value and b is the norm of the Burgers' vector of usual glide dislocations.

The RCI data used here are collected to study the dislocations cells in cm-Si ingots. The FWHM maps were discussed in [9, 14] in terms of local lattice distortion between cells. Here, the focus is on the PP measurements that give local quantitative values to be compared to the misorientation measurements performed by <001> XRD. The FWHM maps are used to assess the presence of dislocations cell network in the studied areas.

3. Results

3.1. (001) orientation gradient measurement by XRD

The misorientation of {001} lattice planes relatively to the sample surface normal as a function of distance to the center of the ingot are plotted in Figure 3 along the two perpendicular X and Y sample axes. For all samples, it is possible to measure θ_x and θ_y along X and Y axes, respectively (Figure 3.a and d). For HG sample, which is cut into sub-areas accordingly to Figure 2.b, additional measurements are performed for θ_x along the Y axis (Figure 3.b) and θ_y along the X axis (Figure 3.c). A similar <001> orientation scan on an unused Cz seed results in a flat one value profile for each θ_x and θ_y only depending on the cutting planes. Here, all <001> orientation components θ_x are contained within the [+0.8°; +2.0°] range and θ_y within the [-0.1°; -0.9°] range thus extending over a range much wider than our accuracy (±0.1 degree).

Looking first at θ_x results along X axis in Figure 3.a, a linear trend variation along the scan directions X is observed for the three samples revealing the presence of crystal misorientation as a function of the distance from the center of the ingot. Surprisingly, the absolute values of θ_x and the slope $\Delta\theta_x/\Delta x$ do not vary monotonically with ingot height. The sample taken at a position close to the start of growth shows lower values for both absolute value of the misorientation and slope. Keeping aside the absolute values which are more difficult to compare, the orientation gradients (slope $\Delta\theta_x/\Delta x$) are compared. It appears that the seed orientation gradient falls in between the gradient at the start of growth and at half growth meaning that reorganization of the crystal structure along the ingot width and height is taking place at some stages of crystal growth or cooling.

A somewhat similar behavior is found in Figure 3.d for θ_y measurements along the Y axis. Here again θ_y and the slope $\Delta\theta_y/\Delta y$ do not evolve monotonically with the ingot height. An exception to the linear trend for θ_y as a function of Y axis is found for sample SG. Here an abrupt change of both the value of θ_y and sign of $\Delta\theta y/\Delta y$ is observed for Y values between 4.5 cm and 7.5 cm. Values for θ_y below 4.5 cm are lower than for S and SG samples as is the case for θ_x along X axis. For Y larger than 7.0 cm, θ_y values and slope lie in between values for S and HG samples of θ_y. This exception to the linear behavior is discussed in §4.1 and seems to be associated to liquid silicon infiltration in between ingot seeds.

θ_x (resp. θ_y) is a rotation around Y axis (resp. X axis). As θ_y scan along X axis of HG sample in Figure 3.c contains much less radial variation (<0.1°) than θ_x, we can assert that for this sample, the rotation of the crystal lattice is mainly a rotation around the Y axis along the X direction. From Figure 3, it is found that average crystal orientation gradients $\Delta\theta_x/\Delta x$ along X direction and $\Delta\theta_y/\Delta y$ along Y direction are significantly larger than $\Delta\theta_y/\Delta x$ and $\Delta\theta_x/\Delta y$ (Table 1). In the HG sample, an orientation gradient of (-0.04 ± 0.01) degree/cm along X axis and a perpendicular orientation gradient of (-0.05±0.01) degree/cm along Y axis are measured. At mid ingot height, Figure 2.b reveals that some sub-grains are present at ingot edge in that sample. No direct relation with sub-grains can be established using only the XRD experiments. However, significant amounts of SGBs are detected by PL at positions where deformation are larger. Tracking growth axis <001> misorientation over large distances (> 10 cm) shows the existence of small crystal rotations with values of about 0.01 degree/cm with, in the end, quite large misorientation due to the long-distance range it applies and to a cumulative effect. From ingot center to the edge, misorientation change in the same grain in the HG sample is approximately $\Delta\theta_x$=0.5° and $\Delta\theta_y$=0.6° along X and Y axis, respectively. As each of those misorientations component θ_x and θ_y are mainly orthogonal, the top left of the sample in Figure 2.b has a misorientation above one degree relatively to the bottom right corner.

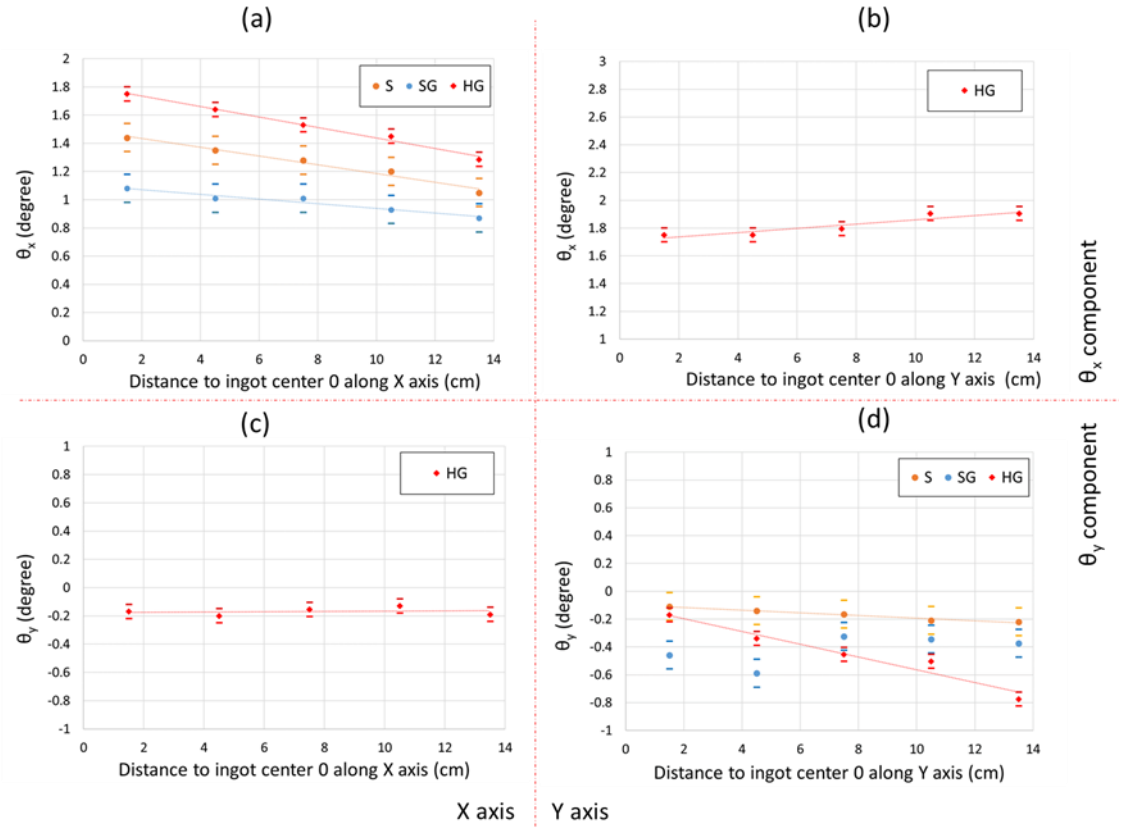

Figure 3: Misorientation relative to <001> as a function of the distance to the center of the ingot along the X and Y axes. θ_x in X direction (a) θ_x in Y direction (b) θ_y in X direction (c) θ_y in Y direction (d). Seed (S), start of growth (SG) and half ingot (HG) labels correspond to ingot heights of 0.7 cm, 1.4 cm and 8.9 cm, respectively.

Table 1: Summary of the average orientation gradients for each orientation component and direction extracted from Figure 3, as a function of the ingot height H. *See Figure 3.d, there are two different slopes over sample length.

H	$d\theta_x/dx$	$d\theta_x/dy$	$d\theta_y/dx$	$d\theta_y/dy$
cm	° /cm	° /cm	° /cm	° /cm
0.7	-0.03 ± 0.02	N.A.	N.A.	-0.01 ± 0.02
1.4	-0.02 ± 0.02	N.A.	N.A.	*
8.9	-0.04 ± 0.01	0.01 ± 0.01	0.00 ± 0.01	-0.05 ± 0.01

For this ingot brick A, the measurements tend to show that {001} plane curvature can be biaxial or axi-symmetrical. Solid/liquid interface shape could be a parameter related to deformations either through interface phenomena or through thermal gradient induced stress in the solid. Here crystal plane curvature is opposite to the interface shape curvature, which is convex. The same method of XRD measurements was applied to other cm-Si samples without SGBs. First, orientation gradients were hardly measurable meaning that cm-Si with low sub-grain amount are not prone to large orientation tilts compared to the one reported in the present manuscript. Second, cm-Si ingots with both concave and convex interface shapes (60kg G2 ingots) were also characterized. No direct relation between melting and solidification interface curvature and crystal orientation gradient curvature sign was found.

The XRD measurements confirm the presence of large-scale plane rotations in seeds of cm-Si as in [19]. Additionally, slight orientation changes at seed / start of growth interface and further increase of the measured orientation changes with ingot growth are observed. Moreover, a general trend for a linear orientation gradient is observed for the main rotations θ_x along X, and θ_y along Y. Deformations can be associated to dislocation networks or linked to the microstructure. In those samples, three types of defects were identified in reference [17]: micro twins, background dislocations, and sub-grains (i.e. dislocations walls). No significant sub-grains are present, from PL and etch pit characterizations in the chosen positions where XRD measurements are performed. Thus, those orientation gradients could be associated either to background dislocation density, either to micro-twins.

3.2. Orientation gradient measurement by RCI

This technique is carried out to investigate the potential relation between crystal plane curvature, micro-twins and background dislocations organized in cells.

On the brick D from the same ingot, 3×3 mm^2 samples were extracted from the wafers and measured by RCI selecting the Si (0 0 4) planes. Two types of maps are presented in Figure 4. First, the FWHM map (Figure 4.a) gives the local plane distortion between cells in degrees. The local deformations are arranged in a cellular form that corresponds to cellular arrays of dislocations. The corresponding peak position map (Figure 4.b) reveals the presence of an orientation gradient from bottom left to the top right of the reconstructed map. A line scan along the white arrow in Figure 4.b shows that the peak position gradient is almost linear (Figure 4.c). On top of the linear trend for the variation of the peak position, abrupt changes of the PP are related to the presence of dislocation cell walls perpendicular to the scan line. Indeed, the position of the abrupt PP changes (see for example the PP variations between P1 and P2) correspond to the dislocation cell walls revealed by the FWHM map. The vertical bands clearly seen on the right

side of Figure 4.a reveal the presence of micro-twins. The corresponding local orientation difference at their level is also revealed on the PP map (Figure 4.b). The micro-twins are not modifying the general trend of the evolution of the crystal orientation presented in Figure 4.c.

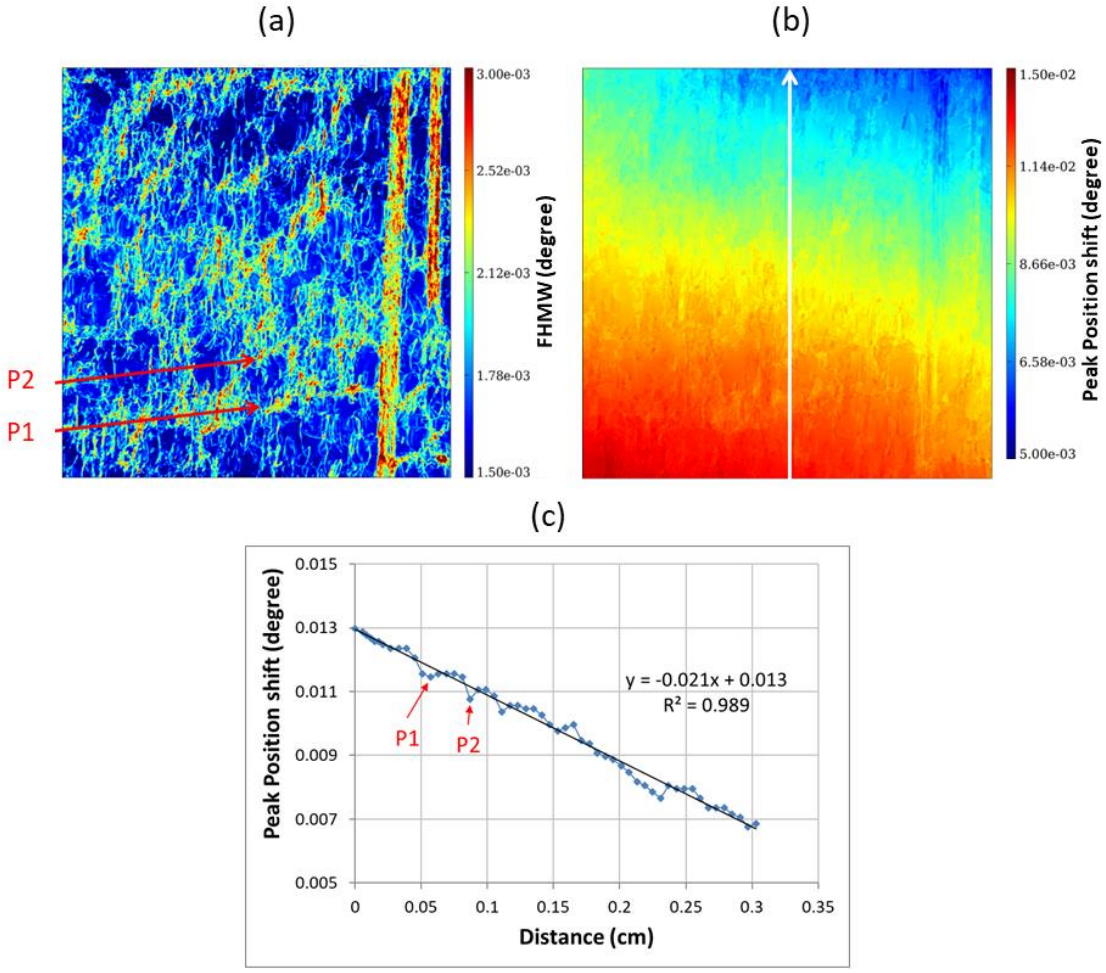

Figure 4: RCI measurements on 3 × 3 mm^2 cm-Si wafer from brick D at ingot height 11 cm; (a) FWHM (full width half maximum) map; (b) corresponding peak position (PP) map; (c) graph corresponding to the line-scan along the white arrow in b). Positions P1 and P2 are indicated in (a) with red arrows. g=004.

4. Discussions

4.1. Singularities in the orientation gradient slope

In this sub-section the measured orientation gradient θ_y sign change observed in Figure 3.d for SG sample and plotted in Figure 5 is discussed. A large view optical image after surface etch pit revelation by chemical attack is also used for the discussion. The etch pit image contrast is inversed (areas with more pits appear whiter). The surfaces measured by XRD are identified as blue rectangular areas. At that scale, individual etch pits are not resolved. However, it is possible to conclude that the pit density decreases from the ingot center (left side) to the ingot edge. At the ingot edge, some sub-grains are also visible as continuous lines forming approximate squares with dislocation walls aligned along <110> directions. In-between the two measurements at 4.5 and 7.5 cm, an orientation change occurs that requires a larger crystal deformation. A 1-2 mm wide linear area inclined to the sample edge with darker contrast indicates that in this linear area, there

is a lower density of dislocation etch pits. The top side of the etch pit image in Figure 5 is also a seed junction area of the pavement. In the S sample, the remaining seed junction is still present and two behaviors are observed along the Y axis. Between the ingot center O and the location of low etch pit area E, the gap in-between seeds is infiltrated by liquid silicon whereas seed junction is not infiltrated after low etch pit area E in Figure 5. A more localized switch between low/high etch pit density areas is also captured in the S sample. Those observations tend to show that the abrupt change in the <001> crystal orientation is related to seed infiltration, maybe through a local change of mechanical boundary limit conditions (free deformation in unfilled seed junction area) of the seeds. One hypothesis to explain our observations is that non-uniform infiltration could generate different local strain conditions at the level of the seeds.

Also surprising is the fact that the abrupt orientation change observed in the SG sample (Figure 5 and blue plot in Figure 3.d) is not present in the S sample neither transferred to the grown-in ingot. In fact, in the measurement on the following HG slab, the main orientation gradient (slope of the red curve in Figure 3.d) is similar to the two point measurements close to center of SG sample and no trace of an orientation discontinuity is captured by our local measurements at ingot height 8.9 cm. Similarly, the slope of θ_y in SG sample far from the center is similar to the one in the seed. A change of (001) orientation gradient slope with a locally higher orientation gradient in seed was found in Krause *et al.* [19] and correlated to a higher dislocation density and lower cell size characterized by etch pit on a vertical plane of similar samples. In [19], it also corresponded to a position upon which sub-grain could develop along ingot height. In this work, the local change of θ_y and of the sign of the slope of $\Delta\theta_y/\Delta y$, is not accompanied by sub-grain development in the upper ingot (see PL imaging insert in Figure 5 taken from the corresponding area in the HG sample). The origin of this abrupt orientation change is unknown to the authors and might not be directly compared to the case studied in [19]. Indeed, it is worth noting that in our sample, area of interest differs from [19] from the fact that the misorientation was voluntarily not measured in areas where SGBs are developing, but instead, in areas free from this kind of defects, in order to be able to measure orientation gradient evolution along width and height. One possible reason why defects are not transmitted to the grown ingot in the form of sub-grains might arise from the time sequence during growth. In fact, it is likely that the deformation in the SG sample took place close to the seed junction after the start of growth and was not propagated to the solid liquid interface.

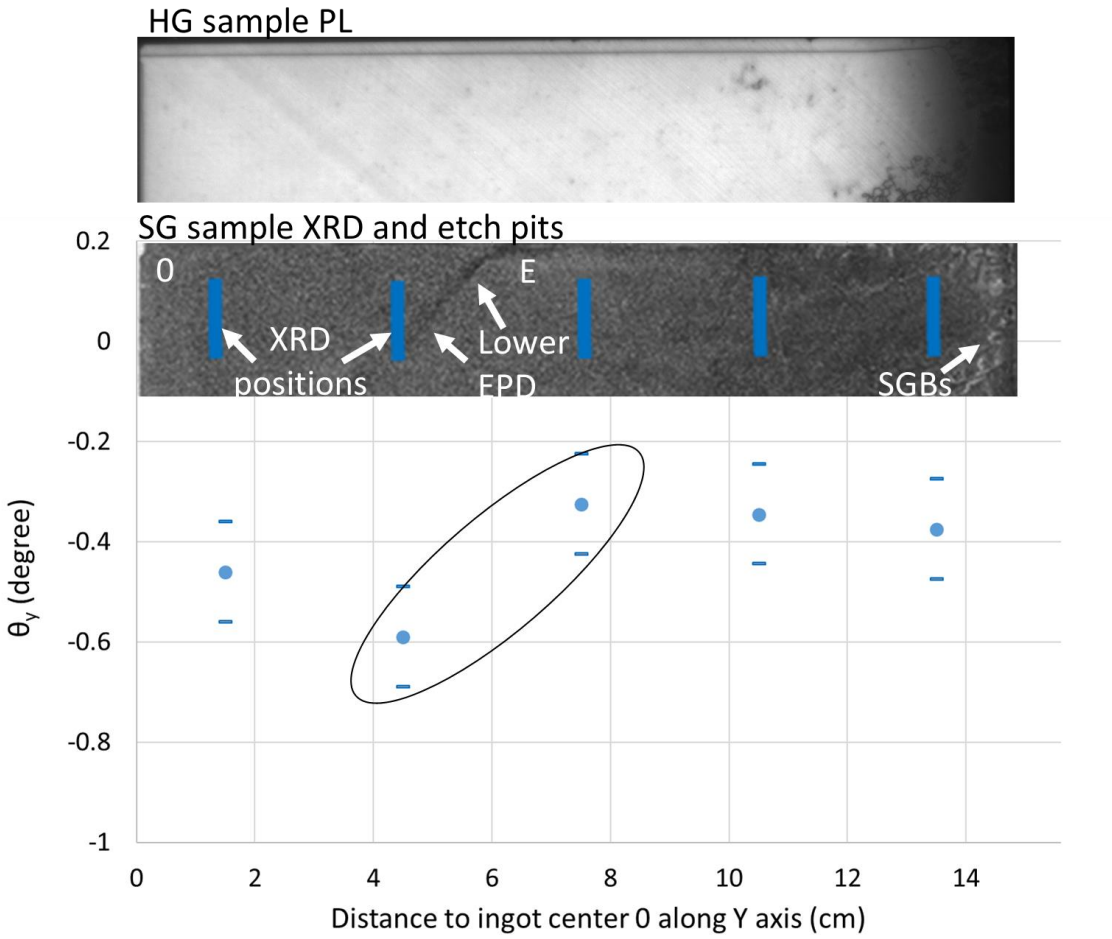

Figure 5: θ_y in Y direction for the SG sample (H = 1.4 cm), etch pit scanner image with XRD measurement positions (blue vertical rectangles) at SG sample surface. Note that the etch pit image has an inverse contrast meaning that areas of higher pit density appear whiter. PL imaging of corresponding area in half growth (HG) sample. The grey horizontal straight line corresponds to a GB induced by a seed junction of the pavement.

4.2. Correlation between large scale and local misorientation measurements in relation to the cellular array of dislocations

(001) orientation variation across cm-Si samples can be described as a linear orientation gradient by both XRD (§3.1) and by RCI (§3.2). Both techniques characterize very different length scales. Orientation gradients extending over 10 cm distance are characterized by XRD on thick samples (> 5 mm) and continuous orientation changes are quantified by RCI over millimeters of wafers samples with angular precision of 2.10^{-4} degree. Given the lower accuracy of the XRD system, the crystal orientation gradients can be measured by XRD only by the cumulative effect of the gradient over the large grain distance. In Figure 6, both measured (001) orientation gradients are compared as a function of the ingot height. Both gradients measured by both techniques on very different scales are of the same order of magnitude between 10^{-2} and 10^{-1} degree/cm. As measurements are performed on similar but neighboring brick, a one to one correlation is not expected.

Interestingly, the fact that both measurements are of same order of magnitude suggests that the background dislocations, organized in cellular network as checked by RCI FWHM results

(§3.2), can be at the origin of the orientation gradient at large distance. In our sample consisting of one large grain, it results in relatively large misorientations of more than one degree between domains belonging to the same grain for the only slab HG.

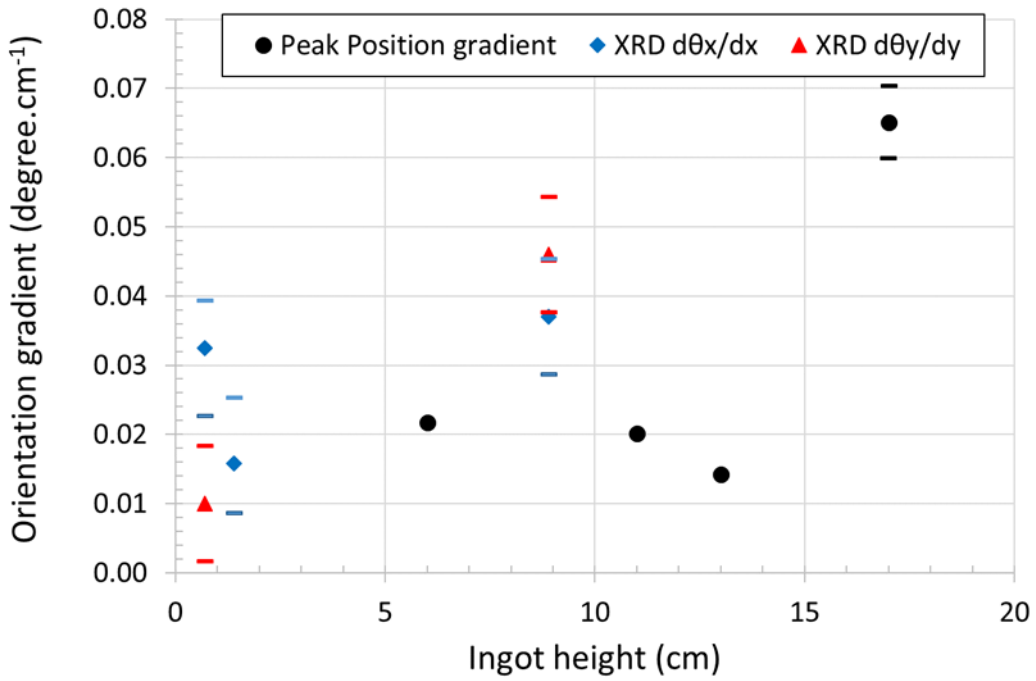

Figure 6: Plot of the average large-scale orientation gradients $\Delta\theta_x/\Delta x$ and $\Delta\theta_y/\Delta y$ measured on brick A samples compared to the peak position evolution measured by RCI on wafer samples (3 × 3 mm^2) from brick D as a function of the ingot height.

Considering sub-grain multiplication from bottom to the top of cm-Si or multi-crystalline (mc-Si) ingots the assumption of an almost perfect, static crystal around sub-grains, implies that those are probably self-multiplying with little interactions with the perfect main crystal. Nevertheless, interactions are mandatory in proposed models [25] and some mobile dislocations interactions with SGBs walls were observed by TEM [18]. This work might slightly change the perspective as we characterize frozen-in crystal orientation changes over: large distance, several sample axes and along ingot height. Considering the epitaxy over a sub-grain surface, the tilt of the surrounding grain with height surely requires SGB properties evolution with height. In other words, orientation change of the bulk of the grains might be connected to the not well-known sub-grain multiplication and densification mechanisms with ingot height.

From a photovoltaic application perspective, the defects in the measured areas do not have a strong impact on the PV efficiency. Indeed, background dislocations in cellular form are hardly captured by carrier lifetime measurement techniques due to a much smaller effect on lifetime than denser sub-grains. Recently, µ-PL was used to characterize defects in particular, sub-grains and dislocations, in silicon ingots [26, 27]. P. Krenckel [27] observed by µPL a cm-Si monocrystalline area containing dislocations cells and found that the cellular dislocation structure is recombination active to some extend but also conclude that it is unclear if it could limit the material quality for solar cells. Nevertheless, several properties of sub-grains deleterious for the PV properties might be underlined in the view of this new result. For (001) cm-Si growth, the number of dislocations in sub-grain domains are increasing in two ways: by increasing the number of SGBs (walls) and

by densifying the dislocations constituting the grain boundaries (increase of misorientation of grain boundaries by rotation about <001> growth axis [10]). In ref [18], a sub-grain domain visible by PL on a vertical section was shown to rotate at a rate of 0.12°/cm about the <001> growth axis. Axis rotation differs in SGB from the one measured in the cellular area. Nevertheless, both crystal rotation in this SGB and the measured horizontal large-scale orientation gradient can be considered of similar order of magnitude (measurement in [18] was made toward the top of ingot). In this work, Figure 6 shows that the orientation gradient increases with height. Additionally, TEM analysis [18] shows that dislocations forming sub-grains in <001> cm-Si are <001> edge dislocations (Lomer type similar to [28]) and lead to sub-grain lattice rotation about <001>. Such dislocations might be formed by elastic reaction of mobile dislocations belonging to different slip planes [18]. The junctions of deformed domains between the cellular and the sub-grain structure are of peculiar importance to check a potential relation to electrically active SGB structure formation. The time at which each defect is formed is a key parameter in this analysis. Sub-grains are believed to be grown-in defects, propagated and multiplied at the solid/liquid (S/L) interface whereas dislocations organized in cells are supposed to have been mobile dislocations frozen-in at some time upon cooling [29].

The growth over FZ seed and cm-Si seed were compared during the heating and growth process through in-situ and post-growth characterization [30]. The presence of sub-grains with misorientations up to 3° was observed in the regrown part of the cm-seeded sample whereas such behavior was not observed in the regrown part of similar experiments performed with seeds issued from zone melting. It was deduced from observations in [30] that the cellular dislocation network, present in cm-Si used as a seed, must carry some kind of deformation in relation with the SGB generation. Here we go further by characterizing a large-scale deformation in the form of an orientation gradient that can extend over two different axis. Nevertheless, a clear understanding of physical relation between dislocation cell network and SGB remains an open question.

4.3. Orientation gradient and equivalent geometrically necessary dislocations

In this sub-section, the geometrically necessary dislocations (GND) are evaluated to accommodate the measured orientation gradients and their evolution along ingot height is discussed. The FWHM map obtained from RCI (see §3.2) gives local distortion which is not necessarily associated to an organization of the dislocations. This is the non-geometrically necessary dislocations and measures somehow the required density to accommodate distortion with dislocations having possibly Burgers' vectors in opposite directions. On the contrary, the presence of the orientation gradient about <001> can be modelled by an ordering of dislocations at large scale with a summing up effect of dislocations having the same sign of their Burgers' vector edge component. A density of geometrically necessary dislocations can be estimated from the orientation gradient measured by XRD and by RCI peak position values for angle variation lower than 1° by:

$$\rho \sim 2\theta/xb \qquad (3)$$

where θ/x is the orientation gradient and b is the norm of the Burgers's vector [31].

Results of GND estimated from equation (3) are summarized in table 2 for the main deformation θ_x along X axis for the three samples characterized by XRD and for one sample characterized by RCI. The relative trends between samples are well captured here and as for figure 6, the more precise RCI peak position analysis comforts the XRD ones. From table 2, it follows that the GND density required to accommodate measured orientation gradients are in the order of some 10^4 cm^{-2}. This is in fairly good agreement with literature for best quality areas from electrical point of view in cm-Si.

Table 2: Summary of the estimated GND density from equation (3).

Ingot height	<001> orientation gradient	Estimated GND
cm	°/cm	cm^{-2}
0.7 (XRD)	-0.03 ± 0.02	~ 3.10^4
1.4 (XRD)	-0.02 ± 0.02	~ 2.10^4
8.9 (XRD)	-0.04 ± 0.01	~ 4.10^4
11 (RCI)	0.021 ± 0.001	~ 2.10^4

Looking first at the S sample, post-growth dislocations density in those seeds (> 10^5 cm^{-2} [17]) is significantly over calculated GND (3.10^4 cm^{-2}). Therefore, there are far enough dislocations in seeds to explain the presence of a crystal lattice tilt. Moreover, a majority of dislocations in seeds does not contribute to the main deformation along the X axis (θ_x). At the start of growth from the seed, the difference between dislocation density in seeds and GND required to accommodate the orientation gradient in the seed can be a first source of reduction of the density of dislocations at seed / growth interface in cm-Si ingots whereas further discussions on the mechanisms are needed [17, 19]. It was found by simulations of a G2 cm-Si ingot process [32], that the thermal stress in seeds is high at the start of melting step, minimum at the start of growth and then increases during crystal growth because of radial heat flow toward solid silicon. The decrease of geometrically necessary dislocation density at start of growth could fit with this stress decrease between melting and start of growth. Nevertheless our results do not reveal a significant increase of GND density with ingot height and thus with increasing stress during growth. To discuss it further, we would need more information on the time sequence of orientation gradient defect formation. In-situ observation of silicon growth may give fruitful additional information there. In such experiments, before the growth starts on the seed, in the course of melting, and at the very start of growth, the surface of remaining seeds close to S/L interface is a location of active dislocation movements [33, 34]. Additionally, a darker contrast in the topographic images is also observed at the seed growth interface during those in-situ experiments, thus revealing a localized stress field around the seed / growth interface [34]. There is a possibility that reorganization of dislocations in seeds in the vicinity of the S/L interface and at the start of growth could provide the mechanism for the density reduction and orientation gradient evolution at the large grain scale due to the induced high dislocation mobility. Anyhow, a mechanism must be responsible to the fact that between S and SG samples, the crystal is tilting with a dependence on distance from the ingot center.

5. Conclusions

Crystal deformation measurements relatively to the [001] growth axis are performed on cm-Si ingot samples by XRD (θ/2θ) over large scale and by RCI. XRD reveals the presence of orientation gradients in the seed, at the start of growth and at mid ingot height. Orientation

gradients up to (0.05 ± 0.02) degree/cm extending over 12 cm inside the single cast-mono grain are measured. It is essential to note that within this area investigated by XRD, no significant electrical defects are visible from MWPCD and PL mappings. Nevertheless, dislocations are present and organized in cells. The measured large-scale orientation gradient is quite continuous and constant over each sample axis. One exception with a localized change of slope of the deformation field inside the sample at start of growth is associated with the infiltration of silicon in between seeds. Surprisingly, this higher deformation volume is neither captured by XRD in the seed nor transmitted up in the ingot as a local deformation or sub-grain appearance. By RCI analysis, an orientation gradient of the {001} planes over 3 mm wide samples can also be measured. This gradient is attributed to the presence of a cellular dislocation network and its linear trend has been confirmed with high accuracy. Localized disruptions in the linear trend can be related to the presence of the dislocation walls perpendicular to the orientation gradient scan direction and to micro-twins.

The misorientation between individual cells was previously believed to be a localized misorientation between unit dislocation cells quantified by RCI FWHM without taking into account a large-scale order. In this work, (001) XRD large scale misorientation measurements are compared to more localized and much more precise RCI measurements on the neighboring brick. The fairly good correlation strongly suggests that background dislocations in a cellular form can create the observed organized orientation gradient over large distance. In our sample consisting of one grain, it results in relatively high misorientations between domains belonging to the same grain (greater than one degree) by summing two perpendicular deformations over two perpendicular horizontal axes.

The geometrically necessary dislocation (GND) density to accommodate the measured orientation gradients are evaluated in the order of some 10^4 cm^{-2} which corresponds to experimental data in the literature in regions of re-growth from seeds without sub-grains in cm-Si. For seeds, post-growth dislocation density is significantly higher than the calculated GND. The fact that a majority of seed dislocations does not contribute to its main deformation may be one significant parameter influencing the reduction of dislocations at seed re-growth interface during cm-Si seeding process.

An enthusiastic perspective of the present work would be to investigate whether the orientation gradients measured in the cm-Si grain are connected to the SGBs domains through misorientation mappings around sub-grains domains. For this, a larger scale RCI on complementary vertical and horizontal sample fields might be the ideal tool to investigate in depth potential relations between orientation gradients in the area where dislocations cells are present as well as the sub-grain domains. In-situ studies could also contribute to explain the transmission of dislocations at the S/L interface and the dynamics of sub-grain formation.

Author contributions

Etienne Pihan: Conceptualization, Methodology, Investigation, Writing - Original Draft, Visualization, **Mickael Albaric:** Conceptualization, Methodology, Investigation, Writing - Review & Editing, **Gabrielle Regula:** Investigation, Writing - Review & Editing, **Nathalie Mangelinck-Noël:** Conceptualization, Methodology, Investigation, Writing - Review & Editing

Acknowledgements

The authors would like to thank the team of the ESRF BM05 beamline for its support and in particular, Thu Nhi Tran and José Baruchel.

Funding

RCI were performed at ESRF by T.N. Tran-Thi and V.A. Oliveira in the frame of a CEA funded Carnot project/SiDeRA.

References

[1] N. Stoddard, B. Wu, I. Witting, M.C. Wagener, Y. Park, G.A. Rozgonyi, R. Clark, Casting Single Crystal Silicon: Novel Defect Profiles from BP Solar's Mono2 TM Wafers, Solid State Phenomena 131-133 (2008) 1-8. https://doi.org/10.4028/www.scientific.net/SSP.131-133.1

[2] A. Jouini, D. Ponthenier, H. Lignier, N. Enjalbert, B. Marie, B. Drevet, E. Pihan, C. Cayron, T. Lafford, D. Camel, Improved multicrystalline silicon ingot crystal quality through seed growth for high efficiency solar cells, Progress in Photovoltaics: Research and Applications 20 (2012) 735-746. https://doi.org/10.1002/pip.1221

[3] M. Trempa, C. Reimann, J. Friedrich, G. Müller, D. Oriwol, Mono-crystalline growth in directional solidification of silicon with different orientation and splitting of seed crystals, Journal of Crystal Growth 351 (2012) 131-140. https://doi.org/10.1016/j.jcrysgro.2012.04.035

[4] V.A. Oliveira, B. Marie, C. Cayron, M. Marinova, M.G. Tsoutsouva, H.C. Sio, T.A. Lafford, J. Baruchel, G. Audoit, A. Grenier, T.N. Tran Thi, D. Camel, Formation mechanism and properties of twinned structures in (111) seeded directionally solidified solar grade silicon, Acta Materialia 121 (2016) 24-36. https://doi.org/10.1016/j.actamat.2016.08.063

[5] V.A. Oliveira, M. Rocha, A. Lantreibecq, M.G. Tsoutsouva, T.N. Tran-Thi, J. Baruchel, D. Camel, Cellular dislocations patterns in monolike silicon: Influence of stress, time under stress and impurity doping, Journal of Crystal Growth 489 (2018) 42-50. https://doi.org/10.1016/j.jcrysgro.2018.03.002

[6] V.A. Oliveira, H.C. Sio, A. Faujour, L. Piot, A. Chabli, D. Camel, Recombination Activity of 2D Extended Defects in Monolike Silicon, Energy Procedia 92 (2016) 755-763. https://doi.org/10.1016/j.egypro.2016.07.055

[7] M.G. Tsoutsouva, V.A. Oliveira, D. Camel, T.N. Tran Thi, J. Baruchel, B. Marie, T.A. Lafford, Segregation, precipitation and dislocation generation between seeds in directionally solidified mono-like silicon for photovoltaic applications, Journal of Crystal Growth 401(0) (2014) 397-403. https://doi.org/10.1016/j.jcrysgro.2013.12.022

[8] M.G. Tsoutsouva, V.A. Oliveira, D. Camel, J. Baruchel, B. Marie, T.A. Lafford, Mono-like silicon ingots grown on low angle misoriented seeds: Defect characterization by synchrotron X-ray diffraction imaging, Acta Materialia 88(0) (2015) 112-120. https://doi.org/10.1016/j.actamat.2015.01.012

[9] A. Autruffe, V. Stenhjem Hagen, L. Arnberg, M. Di Sabatino, Dislocation generation at near-coincidence site lattice grain boundaries during silicon directional solidification, Journal of Crystal Growth 411 (2015) 12-18. https://doi.org/10.1016/j.jcrysgro.2014.10.054
[10] K.E. Ekstrøm, G. Stokkan, R. Søndenå, H. Dalaker, T. Lehmann, L. Arnberg, M. Di Sabatino, Structure and dislocation development in mono-like silicon, physica status solidi (a) 212(10) (2015) 2278-2288. https://doi.org/10.1002/pssa.201532105
[11] A. Autruffe, L. Vines, L. Arnberg, M. Di Sabatino, Coincident site lattice bi-crystals growth—Impurity segregation towards grain boundaries, Journal of Crystal Growth 416 (2015) 8-11. https://doi.org/10.1016/j.jcrysgro.2015.01.009
[12] M. Trempa, C. Reimann, J. Friedrich, G. Müller, L. Sylla, A. Krause, T. Richter, Investigation of iron contamination of seed crystals and its impact on lifetime distribution in Quasimono silicon ingots, Journal of Crystal Growth 429 (2015) 56-62. https://doi.org/10.1016/j.jcrysgro.2015.08.004
[13] M. Trempa, C. Reimann, J. Friedrich, G. Müller, A. Krause, L. Sylla, T. Richter, Influence of grain boundaries intentionally induced between seed plates on the defect generation in quasi-mono-crystalline silicon ingots, Crystal Research and Technology 50(1) (2015) 124-132. https://doi.org/10.1002/crat.201400226
[14] V. A. Oliveira , Influence of processing parameters on the generation and propagation of electrically active crystalline defects in monolike silicon (Ph.D. thesis), Université Grenoble Alpes (2016). http://www.theses.fr/2016GREAI021
[15] A. Lantreibecq, Détermination de la nature et de l'origine des défauts cristallins dans le silicium monolike (Ph.D. thesis), Université de Toulouse (2018). http://thesesups.ups-tlse.fr/4222/
[16] K. Jiptner, B.Gao, H. Harada, Y. Miyamura, M. Fukuzawa, K. Kakimoto, T. Sekiguchi, Thermal stress induced dislocation distribution in directional solidification of Si for PV application, Journal of Crystal Growth, Volume 408, 2014, Pages 19-24. https://doi.org/10.1016/j.jcrysgro.2014.09.017
[17] A. Lantreibecq, M. Legros, N. Plassat, J.P. Monchoux, E. Pihan, Spatial distribution of structural defects in Cz-seeded directionally solidified silicon ingots: An etch pit study, Journal of Crystal Growth 483 (2018) 183-189. https://doi.org/10.1016/j.jcrysgro.2017.11.024
[18] A. Lantreibecq, J.-Ph. Monchoux, E. Pihan, B. Marie, M. Legros, Subgrains, micro-twins and dislocations characterization in monolike Si using TEM and in-situ TEM, Materials Today: Proceedings 5 (2018) 14732–14747. https://doi.org/10.1016/j.matpr.2018.03.063
[19] A. Krause, L. Sylla, D. Oriwol, Plastic deformation as an origin of dislocations in cast mono, Energy Procedia 92 (2016) 833-838. https://doi.org/10.1016/j.egypro.2016.07.082
[20] R. Cabal, N. Enjalbert, E. Pihan, N. Plassat, G. Fortin, L. Bounaas, S. Dubois, CRYSTALMAX Silicon for High Efficiency / Low-Cost Solar Cells, Proceedings of the 32nd European Photovoltaic Solar Energy Conference and Exhibition, Munich (2016), pp. 285-288, https://doi.org/10.4229/EUPVSEC20162016-2BO.1.1
[21] J. Huang, S. Yuan, X. Yu, D. Yang, Growth and Defects in Cast-Mono Silicon for Solar Cells: A Review. Phys. Status Solidi A 2200448, (2022). https://doi.org/10.1002/pssa.202200448
[22] A. Philip, J. Meyssonnier, R.T. Kluender, J. Baruchel, Three-dimensional rocking curve imaging to measure the effective distortion in the neighbourhood of a defect within a crystal: an ice example., J. Appl. Crystallogr. 46 (2013) 842–848. https://doi.org/10.1107/S002188981300472X
[23] M.G. Tsoutsouva, V.A. Oliveira, J. Baruchel, D. Camel, B. Marie, T.A. Lafford, Characterization of defects in mono-like silicon for photovoltaic applications using X-ray Bragg

diffraction imaging, J. Appl. Crystallogr., 48 (2015), pp. 645-654. https://doi.org/10.1107/S1600576715004926
[24] P.B. Hirsch, Mosaic structure, (1956) Progress in Metal Physics, 6 (C), pp. 236-339. https://doi: 10.1016/0502-8205(56)90008-9
[25] D. Oriwol, E.-R. Carl, A.N. Danilewsky, L. Sylla, W. Seifert, M. Kittler,H.S. Leipner, Small-angle subgrain boundaries emanating from dislocation pile-ups in multicrystalline silicon studied with synchrotron white-beam X-ray topography, (2013) Acta Materialia, 61 (18), pp. 6903-6910. https://doi.org/10.1016/j.actamat.2013.08.002
[26] H. T. Nguyen, F. E. Rougieux, F. Wang, H. Tan and D. Macdonald, "Micrometer-Scale Deep-Level Spectral Photoluminescence From Dislocations in Multicrystalline Silicon," in IEEE Journal of Photovoltaics, vol. 5, no. 3, pp. 799-804, May 2015, doi: 10.1109/JPHOTOV.2015.2407158.
[27] P. Krenckel, Y. Hayama, F. Schindler, T. Trötschler, S. Riepe, N. Usami, Propagation of Crystal Defects during Directional Solidification of Silicon via Induction of Functional Defects. Crystals 2021, 11, 90. https://doi.org/10.3390/cryst11020090
[28] J. Bauer, A. Hahnel, P. Werner, N. Zakharov, H. Blumtritt, A. Zuschlag, O. Breitenstein, Recombination at Lomer Dislocations in Multicrystalline Silicon for Solar Cells, IEEE J. Photovolt., 6 (1) (2016), pp. 100-110. https://doi.org/10.1109/JPHOTOV.2015.2494680
[29] K. Jiptner, M. Fukuzawa, Y. Miyamura, H. Harada, K. Kakimoto, T. Sekiguchi, Evaluation of residual strain in directional solidified mono-Si ingots, Phys. Status Solidi C, 10 (2013), p. 141. https://doi.org/10.1002/pssc.201200884
[30] M. Becker, E. Pihan, F. Guittonneau, L. Barrallier, G. Regula, H. Ouaddah, G. Reinhart, N. Mangelinck-Noël, Investigation of subgrains in directionally solidified cast mono-seeded silicon and their interactions with twin boundaries, Solar Energy Materials and Solar Cells, 2020, 218, pp.110817. https://doi.org/10.1016/j.solmat.2020.110817
[31] X. Zhang, L. Zhang, S. Mironov, R. Xiao, L. Guo, T. Huang, Effect of crystallographic orientation on structural response of silicon to femtosecond laser irradiation, Applied Physics A (2021) 127:196. https://doi.org/10.1007/s00339-021-04341-y
[32] A. Lantreibecq, M. Legros, D. Pelletier, J.P. Monchoux, E. Pihan, Thermomechanical Stress Modelling during Melting and Solidification of a Monolike Ingot Process, 33rd European Photovoltaic Solar Energy Conference and Exhibition, Amsterdam (2017), pp505-508. https://doi.org/10.4229/EUPVSEC20172017-2AV.1.15
[33] S.W. Neves Dias, M. Becker, H. Ouaddah, I. Périchaud, G. Reinhart, N. Mangelinck-Noël and G. Regula (2022), Dislocation Dynamics in Monocrystalline Si near the Melting Point Studied in Situ by X-Ray Bragg Diffraction Imaging. Phys. Status Solidi B 2100594. https://doi.org/10.1002/pssb.202100594
[34] M. Becker, G. Regula, G. Reinhart, E. Boller, J.-P. Valade, A. Rack, P. Tafforeau, N. Mangelinck-Noël, Simultaneous X-ray radiography and diffraction topography imaging applied to silicon for defect analysis during melting and crystallization, J. Appl. Crystallogr., 52 (2019), pp. 1312-1320, https://doi.org/10.1107/S1600576719013050